A Novel Reconfigurable Bandpass Filtering Antenna for IoT Communication Applications

Vamsee K. Allam, Boddapati T. P. Madhav*, **Tirunagari Anilkumar, and Suman Maloji**

Abstract—This paper presents a novel reconfigurable filtering antenna with three tunable states used for IoT applications. The frequency reconfigurability is achieved using the combination of a hairpin filter and an open loop filter in the structure with the switching of p-i-n diodes. The open-loop filter structure provides two narrow band states at 2.4 GHz and 7.8 GHz, and the hairpin filter provides a single narrow band state at 10.4 GHz. The frequency reconfiguration is obtained without compromising the compact size of the designed circuit along with the targeted frequency bands at lower WLAN (2.47 GHz), WiMAX (3.42 GHz), INSAT C-band (7.18 GHz), fixed/mobile satellite service in X-band (8.4 GHz), direct broadcast service in Ku-band (12.14 GHz) applications. The prototype is constructed on an FR4 substrate and tested for validation in an anechoic chamber. The designed antenna provides excellent radiation characteristics and considerable gain at resonant frequencies. The proposed reconfigurable antenna is also tested using the CDAC Cmote device in the real-time environment and found more suitable for the IoT based communication applications.

1. INTRODUCTION

Nowadays, reconfigurable antennas are being used in distinct areas like Internet of Things (IoT) applications, wireless network security, cognitive radio, mobile and satellite communications. The development of wireless communication systems also increases rapidly, hence it is necessary to provide small size and multiband antennas for IoT applications. IoT will provide a platform to allow big data transfer mechanism and communication between people and devices, which provide high quality of life in society [1]. IoT is a worldwide network that provides a platform allowing big data transfer and connection between people and things. To acquire good communication, the antennas connecting to IoT are needed to be small, cost-effective, energy efficient to operate in the different bands for WLAN (IEEE 802.11 a/b/g/n), GSM (800 MHz, 850 MHz, and 1.9 GHz), Zigbee (IEEE 802.15.4), LTE, WiMAX (IEEE 802.16), etc. [2]. Reconfigurability among such applications is desirable in IoT based communication, which can be achieved through frequency reconfigurable antennas. Many such antennas are proposed in the literature, and some of them are presented here. A new topology based multiband LP-RFID reader antenna is designed by Bashir et al. in [3], and a total UHF-RFID band of 840 MHz to 960 MHz, 2.4 GHz of ISM, and 5.77 GHz SHF band is covered by the antenna. In addition to that, it also covers TV bands (697 MHz to 884 MHz) and GSM band with a −10 dB impedance matching. A frequency reconfigurable bow-tie antenna is designed for WiMAX, Bluetooth, and WLAN applications by T. Li in [4] in which the effective length of the designed antenna is changed by employing p-i-n diodes on the bow-tie arms leading to tunable operating band. Sun et al. in [5] designed a compact reconfigurable patch antenna employed a shorting structure, which can switch among three bands. A reconfigurable circular disc antenna with a p-i-n diode switching able to switch between wideband state

and narrowband state which is proposed by Qin et al. in [6]. Rhee et al. in [7] designed an airborne blade antenna which switched between 30–400 MHz and 960–1220 MHz bands through p-i-n diode switching. A frequency and pattern reconfigurable slotted antenna was designed by Majid et al. in [8] and achieved through incorporating two switches in the slot (for frequency reconfigurable) and three switches in each of the four slits in the ground plane (for pattern reconfigurable). Cai et al. proposed a grid-slotted low-profile frequency reconfigurable antenna in [9], to achieve frequency reconfigurability, and the radiating patch was loaded with two varactors. A compact reconfigurable narrowband microstrip slot antenna was designed in [10], in which the electrical length of the slot was varied through five p-i-n diodes for reconfiguration, and the antenna radiated with a bidirectional pattern. A half annular ring slot frequency reconfigurable antenna was designed with a meandered tuning stub, and four bands were obtained with good tuning in the operating frequency by simply placing switching diodes in [11]. Yang et al. in [12] proposed a frequency tunable microstrip antenna by adding a U-slot on the patch in which matching frequency was varied by adjusting the input reactance. Li et al. proposed a slot-loop varactor-loaded antenna with a tunable matching network (TMN) in [13]. Simorangkir et al. proposed a frequency-reconfigurable and wearable antenna using PDMS-embedded conductive-fabric technology in [14]. The antenna operated with a tuning frequency from 2.3 to 2.68 GHz. Cheung et al. proposed, in [15], a low-profile frequency-tunable slotted antenna with a wide tuning range for cognitive radio applications in which the resonant frequency was tuned from 2.14 to 3.33 GHz by varying the reverse-bias voltage across the varactors. Costa et al. in [16] proposed a low-profile, high impedance surface tunable and steerable antenna. Liang et al. proposed a dual-polarized tunable EBG structure on a thin polyester substrate in [17]. Sam and Zakaria proposed a varactor diodes based tuning element antenna in [18] in which tuning frequency range over 200 MHz was obtained by using varactor diodes. Ge et al. proposed a stacked patch dual-band antenna with frequency reconfiguration in [19] in which the change in the reverse bias voltage in the varactor diodes got tunability from 1.68 to 1.93 GHz at lower band and 2.1 to 2.5 GHz at the higher band. Liu et al. proposed a low profile broadband slot mushroom antenna in [20] in which the impedance matching of the antenna was obtained by changing the feeding slot.

In this paper, we propose a frequency reconfigurable antenna using a combination of an open loop filter and a hair pin band pass filter as shown in Fig. 1. By placing p-i-n diodes at appropriate places, we achieve reconfigurability in the antenna. The designed antenna resonates at 2.47 GHz, 7.18 GHz 12.14 GHz, 3.42 GHz, 14.55 GHz, 8.4 GHz for different switching conditions.
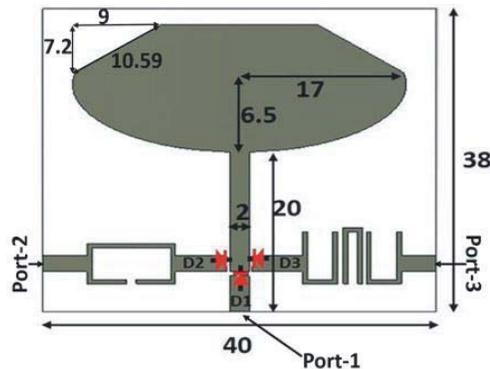

Figure 1. Configuration of the proposed filtering antenna.

The operating bands are more suitable for wireless communication and IoT applications. A brief report of design and analysis of the proposed antenna is presented in this work. Measured and simulated parameters of reflection coefficient (S_{11}), radiation patterns, and surface current distributions are presented. The fabricated antenna is tested practically by connecting antenna to Cmote as a transmitting/receiving antenna and transmits the data from one Cmote to another Cmote. The simulation analysis and optimization of the modelled antenna are done by using time domain solver in the CST Microwave Studio tool.

2. EVOLUTION OF THE ANTENNA

Initially, an elliptical shape structure is considered as a radiating element of the antenna. The antenna is fed with a microstrip line feed, and it is backed by a partial ground plane with the dimension equal to half of the substrate's length. It is designed on an FR-4 substrate with relative permittivity of 4.3 and thickness of 1.6 mm. This design is later modified in iteration-2 by truncating the top corners of the ground plane and leaving the elliptical shape radiator as before. In the third iteration, the upper boundary of the elliptical radiator is truncated, and the ground plane is kept as in Iteration-1, to study the effects of truncating the elliptical radiator. In iteration-4, both the radiating structure and top corners of the ground plane are truncated as shown in Fig. 2. The design of the proposed antenna is based on the truncated structures, which can be applied to the radiating patch and ground plane of the antenna. This results in the evolution of the antenna as the above mentioned four iterations with possible combinations of truncated structures. The radiating patch is truncated by cutting a right-angled triangular portion with side lengths 7.2 mm, 9 mm, 10.59 mm, and the corners of the ground plane are truncated by removing isosceles triangles of side length equal to 6 mm.

(a)   (b)   (c)   (d)
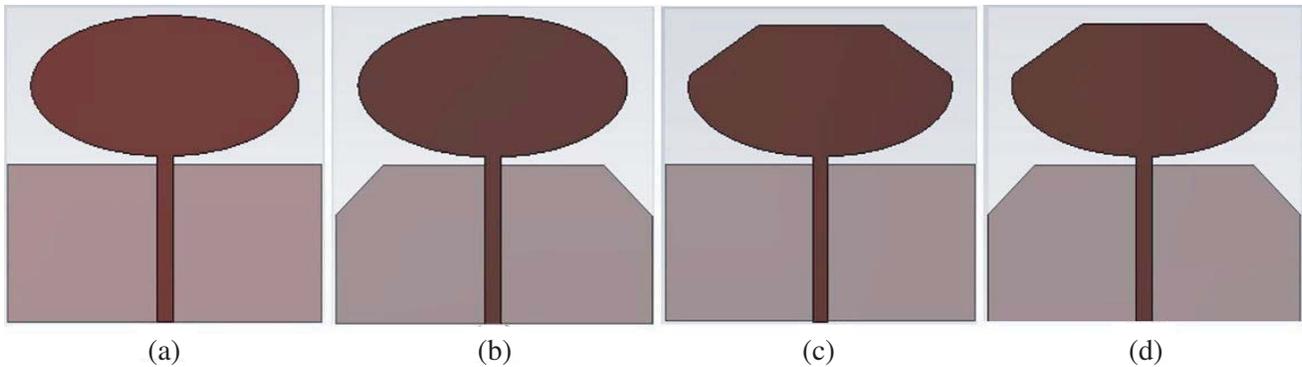
Figure 2. Layouts of the proposed monopole antennas.

The reflection coefficient characteristics for the above iterations is presented in Fig. 3. From the figure one can understand that the antenna iteration-1 and iteration-3 which have no variation in ground plane exhibit dual-band characteristics across 2.8–3.5 GHz and 7.7–9 GHz. The ground plane with corners truncated leads to enhanced bandwidth characteristics in the above-mentioned bands which can be observed from Fig. 3. The combination of truncated patch and ground structures yields considerable reflection coefficient characteristics with enhanced bandwidth.
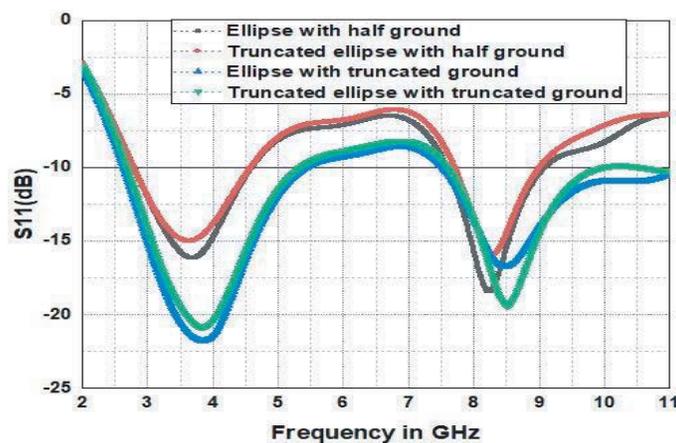
Figure 3. Reflection coefficients of the proposed monopole antennas.

The equivalent circuit model of elliptical microstrip patch antenna is of parallel combination with inductance 'L', resistance 'R', and capacitance 'C'. By taking fringing fields into consideration for the dominant mode TM_{11}, the resonant frequency of the elliptical microstrip patch antenna is [21]

$$f_r = \frac{c\sqrt{q_{11}}}{\pi a e \sqrt{\varepsilon_r}} \tag{1}$$

$$\text{where } q_{11} = 0.847e^2 - 0.0013e^3 + 0.0379e^4$$

where 'e' corresponds to the eccentricity; 'a' is the length of the semi major axis of elliptical patch respectively; and 'c' is the velocity of light.

The input impedance, Z_{in}, of elliptical patch is equivalent to the impedances of R, L, C lumped elements in parallel combination, and it is expressed as

$$\text{Input impedance,} \quad Z_{in} = \frac{1}{\left\{\left(\frac{1}{R}\right) + (jwC) + \left(\frac{1}{jwL}\right)\right\}} \tag{2}$$

For the elliptical patch resonance resistance at feed point can be expressed as

$$R_{in}(\rho' = \rho_0) = \frac{1}{G_t} \frac{J_1^2(K\rho_0)}{J_1^2(Ka_e)} \tag{3}$$

For the elliptical patch antenna, the capacitance is given by

$$C = \frac{Q}{2\pi f R} \tag{4}$$

and inductance is given by

$$L = \frac{R}{2\pi f Q} \tag{5}$$

2.1. Hairpin Filter Design

Before designing the reconfigurable antenna, first we design the bandpass filter for the required bands. Fig. 4(a) shows the hairpin filter structure. The simulated S_{11} is given in Fig. 4(b). It provides narrow-band response at 10.4 GHz. The dimensions of the hairpin filter are given in Table 1.

| (a) | (b) |
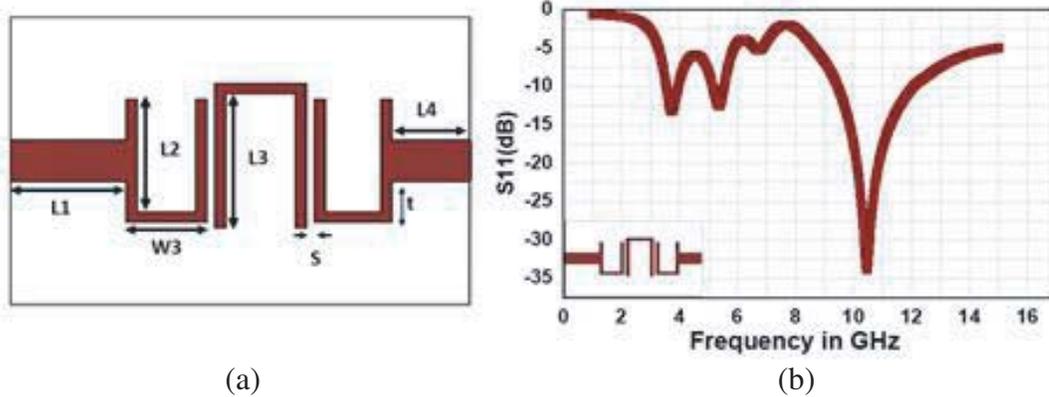
Figure 4. (a) Layout of the Hairpin filter. (b) Simulated S-parameters of the filter.

The design equations of hairpin filter are presented below as mentioned in [22].

$$\frac{J_{01}}{Y_0} = \sqrt{\frac{\pi}{2} \frac{FBW}{g_0 g_1}} \tag{6}$$

Table 1. Dimensions of the filters (UNIT: mm).

| L_1	L_2	W_3	L_3	L_4	L_5	W_5	L_6
5.1	6	3.6	6.5	3.5	4.5	2	9
W_6	L_7	L_8	W_8	t	w	s	g
4	4	5.2	1.35	1.5	0.5	0.35	0.6

$$\frac{J_{J,J+1}}{Y_0} = \frac{\pi FBW}{2} \frac{1}{\sqrt{g_j g_{j+1}}}, \quad j = 1 \text{ to } n-1 \tag{7}$$

$$\frac{J_{n,n+1}}{Y_0} = \sqrt{\frac{\pi}{2} \frac{FBW}{g_0 g_1}} \tag{8}$$

Here 'g_0', 'g_1' represents the elements of a ladder-type lowpass filter prototype with a normalized cutoff frequency of value '1', and the fractional bandwidth of band pass filter is 'FBW'. The characteristic admittances of **J**-inverters are $\mathbf{J_{j\ j+1}}$, and the characteristic admittance of the lines is Y_0.

2.2. Open Loop Filter Design

Figure 5(a) shows the open loop filter. The corresponding simulated S_{11} is given in Fig. 5(b). It produces two narrow bands. One is 2.4 GHz, and the other band is 7.9 GHz. The dimensions of the open loop filter are shown in Table 1.


| (a) | (b) |
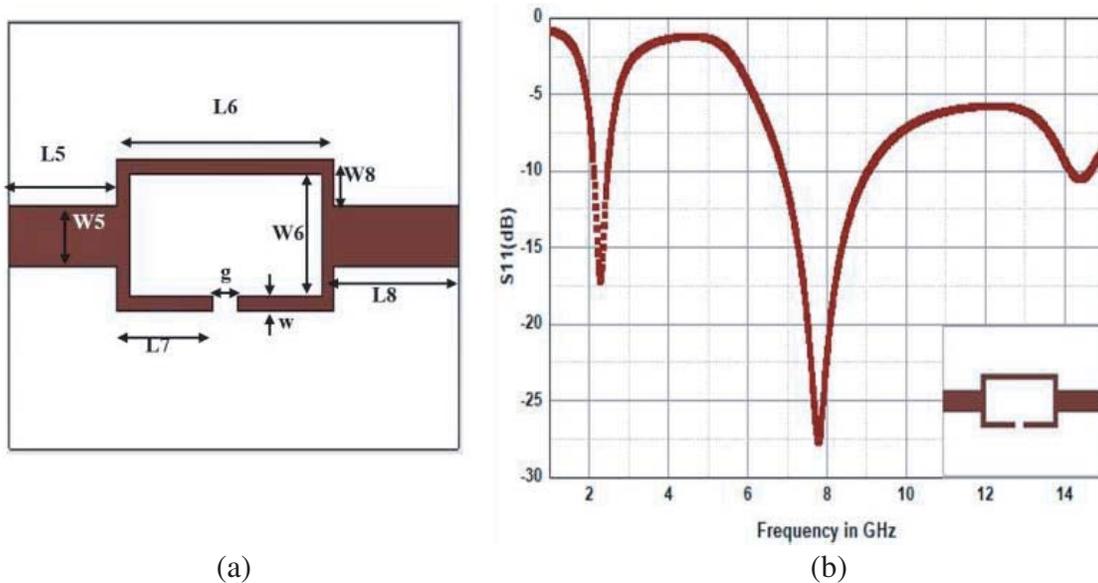
**Figure 5.** (a) Layout of the open loop filter. (b) Simulated S-parameters of open loop filter.

The designing equations of open loop filter are given by center frequency $f_0 = 2.4$ GHz, fractional bandwidth of passband FBW = 0.058, filter order = 3, terminal impedance of passband 1/YA 50 ohm, theta = 45 degrees, and Ya = 1/130 mhos [22].

2.3. Configuration of the Antenna with Bandpass Filters

The open loop filter is connected to the truncated elliptical patch with truncated ground. It is given in Fig. 6(a). The corresponding simulated S_{11} is shown in Fig. 6(b). The antenna operates at two
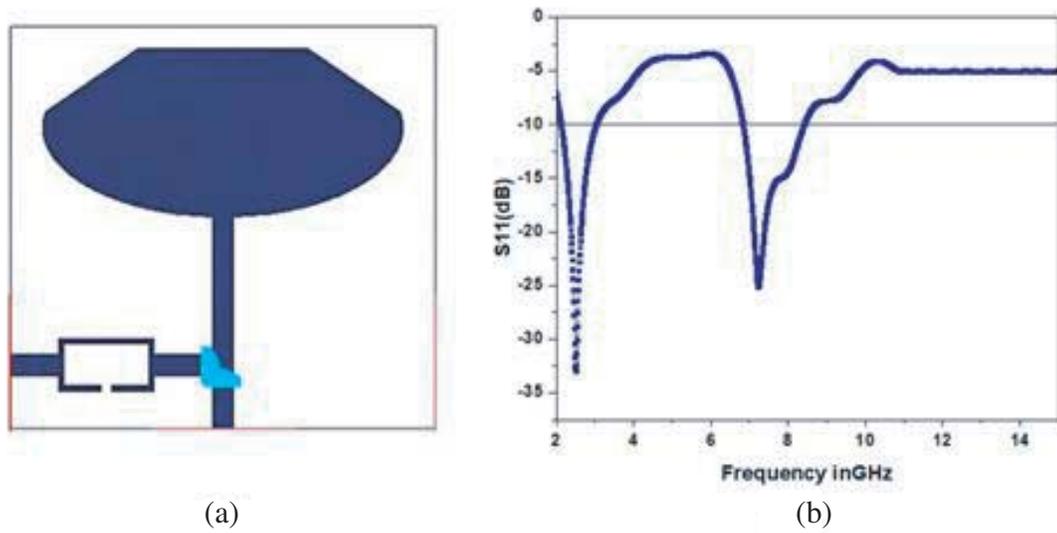
**Figure 6.** (a) Configuration of the antenna with the open loop filter. (b) Simulated S-parameters.
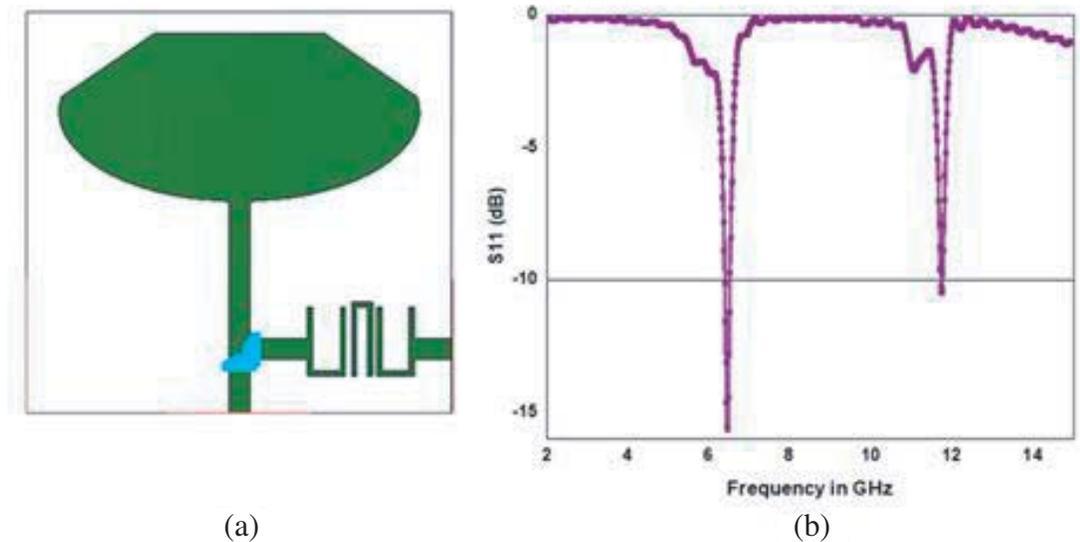
Figure 7. (a) Configuration of the antenna with the Hairpin filter. (b) Simulated S-parameters.

narrow bands 2.4 GHz and 7.4 GHz. Fig. 7(a) shows the layout of the truncated elliptical shape patch antenna with a hairpin filter. It produces 6.4 GHz and 11.9 GHz, respectively, shown in Fig. 7(b). The iterations of the antenna (a) Truncated elliptical monopole patch antenna (b) Monopole antenna with hairpin filter (c) Monopole antenna with open loop filter (d) Monopole antenna with both open loop and hairpin filter are shown in Fig. 8.

3. RECONFIGURABLE FILTERING ANTENNA DESIGN

Figure 1 depicts the whole structure which is integrated with both the hairpin filter and open loop filter to the monopole antenna. Three RF-Ports are composed in the structure, and three diodes D1, D2, D3 are placed at suitable locations. By using p-i-n diodes switching condition, the frequency
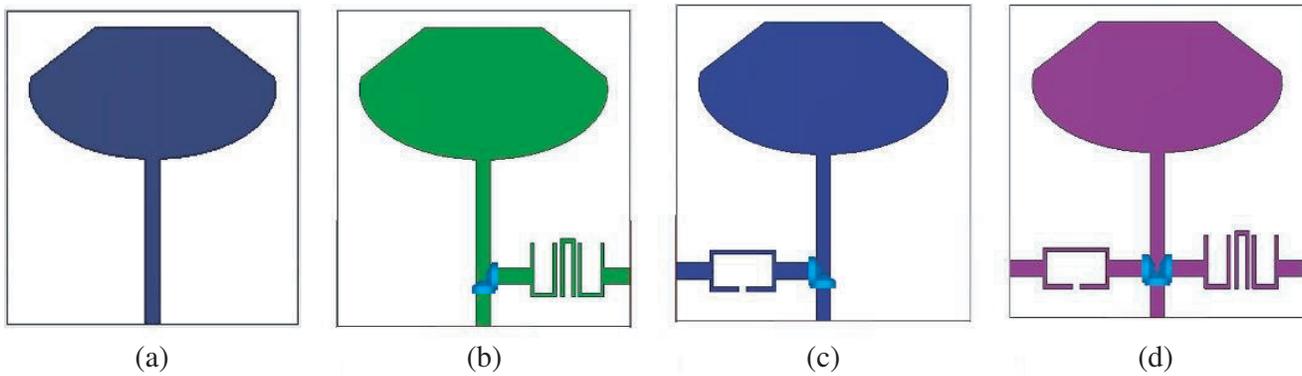
Figure 8. Iterations of the reconfigurable antenna. (a) Iteration-1. (b) Iteration-2. (c) Iteration-3. (d) Iteration-4.
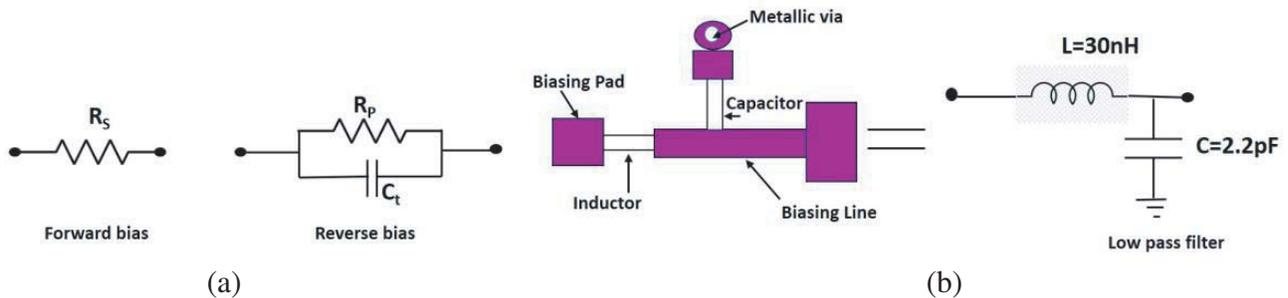

Figure 9. Correspondent circuits for (a) p-i-n diode and (b) reverse biased dc biasing network.

reconfigurability functionality is attained. By using hairpin and open loop filters, we obtain filtering capability in the model. Without increasing the size of the antenna, multi-functional characteristics are obtained. Simulations are performed with the help of CST studio electromagnetic tool.

To achieve frequency reconfigurability, three BAR64-02v numbered p-i-n diodes are used as switching elements. Fig. 9(a) shows the corresponding circuits used in CST simulation software. As per the data sheet, a 4-ohm resistor is used in forward biased condition, and in the reverse bias, a 4 kilo ohm resistor and 0.025 pF capacitor are used in parallel. The DC biasing network for p-i-n diodes in reverse bias is shown in Fig. 9(b).

Three p-i-n diodes D1, D2, D3 are placed at appropriate places at junctions as mentioned above. Diode D1 is placed in feeding line, diode D2 placed beside the open loop filter, and diode D3 placed beside the hair pin filter. BAR64-02v numbered p-i-n diodes are utilized as tuning elements to attain frequency reconfigurability.

With diode-D1 ON and D2, D3 OFF, Port-1 provides an RF signal to the antenna. With D2 ON and D1, D3 OFF, Port-2 provides an RF signal to the antenna. With diode D3 ON and D1, D2 OFF, Port-3 feeds the RF signal to the antenna. With D1 ON, D2 ON and D3 OFF, the antenna operates at three wide bands 2.13–3.0 GHz, 6.8–8.36 GHz, and 12.039–13.14 GHz, respectively. It gives fundamental resonant frequency at 2.47 GHz, and the related S_{11} is given in Fig. 10 in red color. It is also suitable for WLAN operations and IoT applications. With D1 OFF, D2 ON, and D3 ON, the antenna operates at two bands 3.3–3.57 GHz and 14–15.2 GHz. It is shown in Fig. 10 with blue color indication. With D1 ON, D2 OFF, and D3 ON, the antenna operates at only one narrow band 8.3–8.5 GHz as shown in Fig. 10 indicated in black color. By using three diodes, totally eight combinations occur 000, 001, 010, 011, 100, 101, 110, 111, where '0' represents diode OFF condition, and '1' represents diode ON condition. The reflection coefficients for the first four switching conditions are shown in Fig. 11(a), and the last four switching conditions are shown in Fig. 11(b). For the three combinations, 110, 011, 101, the resonant frequencies are 2.47 GHz, 7.18 GHz, 12.14 GHz, 3.42 GHz, 14.55 GHz, and 8.4 GHz. For
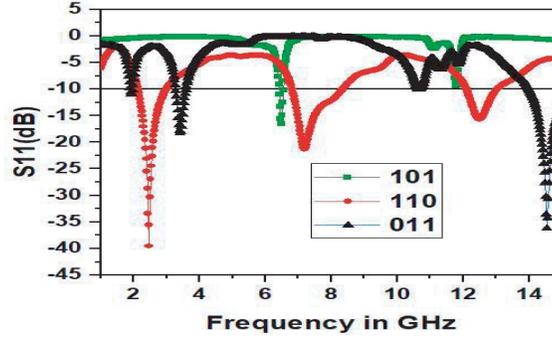
Figure 10. Parametric result for the best reconfigurable targeted frequencies at 2.47 GHz, 7.18 GHz 12.14 GHz, 3.42 GHz, 14.55 GHz, 8.4 GHz for different switching conditions. 0 represents diode OFF condition & 1 represents ON condition.
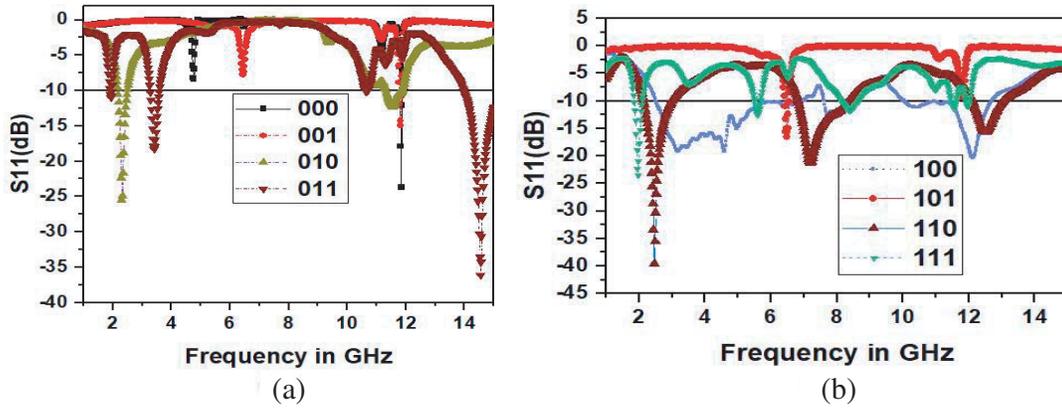

Figure 11. (a) Reflection coefficient for first 4 conditions. (b) Last 4 conditions. 0 represents diode OFF & 1 represents diode ON.

these resonant frequencies, the antenna surface current distributions are plotted in Figs. 12, 13, and 14, respectively. Operating bands and resonant frequencies for different diode conditions are shown in Table 2.
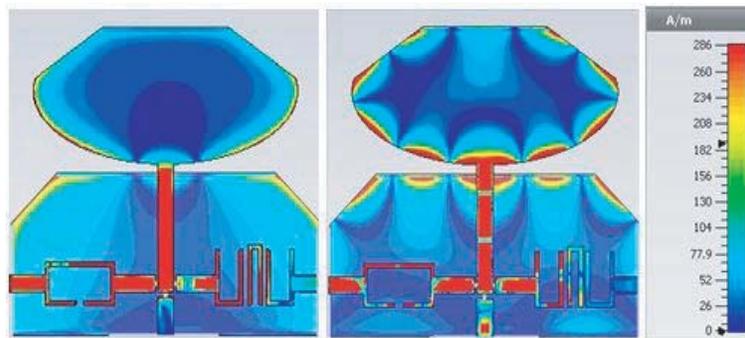
With D1 ON, D2 ON, and D3 OFF, Port-1 feeds an RF signal to the antenna. When Port-1 is excited, it gives three resonant frequencies 2.47 GHz, 7.18 GHz, 12.14 GHz. For all these three frequencies, the surface current distributions and shown in Fig. 12. By looking at the surface current distributions, we can observe good isolation between the ports. The current is not distributed towards Port-3 because diode D3 is OFF. With D1 OFF, D2 ON, and D3 ON, Port-2 feeds an RF signal to the antenna. When Port-2 is excited, it gives two resonant frequencies at 3.42 GHz and 14.55 GHz. For these two frequencies, the simulated surface current distributions can be observed in Fig. 13. The current is distributed over the entire patch, but the current is not distributed towards Port-1 because of D1 OFF. It provides good isolation, and the current is nearly concentrated on the open loop filter only.

Table 2. Operating bands and resonant frequencies for different diode switching conditions.

D1	D2	D3	Operating Bands in GHz	Resonant Frequencies in GHz
ON	ON	OFF	2.13–3.0 / 6.8–8.36 / 12.03–13.14	2.47, 7.18, 12.14
OFF	ON	ON	3.3–3.57 / 14–15.2	3.42, 14.55
ON	OFF	ON	8.3–8.5	8.4
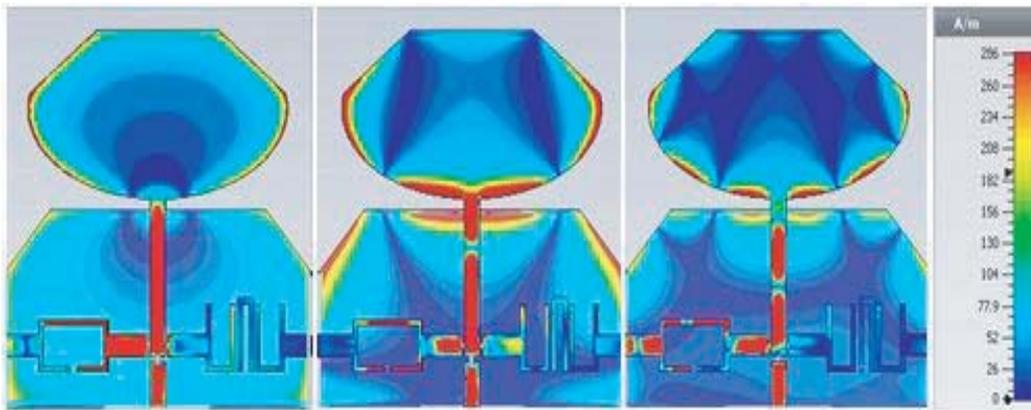
Figure 12. Surface current distribution of the proposed antenna at 2.47 GHz, 7.18 GHz, 12.14 GHz.


Figure 13. Surface current distribution of the proposed antenna at 3.42 GHz, 14.55 GHz.
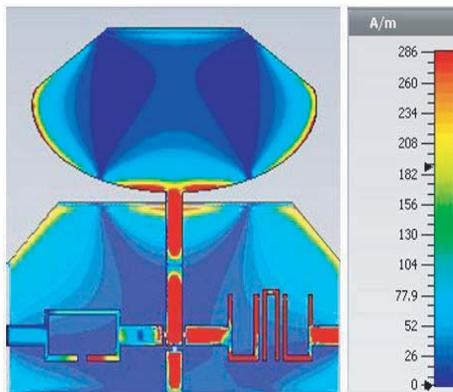
Figure 14. Surface current distribution of the proposed antenna at 8.4 GHz.

With D1 ON, D2 OFF, and D3 ON, Port-3 feeds an RF signal to the antenna. When port-3 is excited, it gives only one resonant frequency at 8.4 GHz. The simulation based current distributions are shown in Fig. 14.

When Port-3 is excited, the surface current is distributed over the entire patch except towards Port-2 because of D2 OFF. It provides good isolation, and the current is nearly concentrated on the hair pin filter.

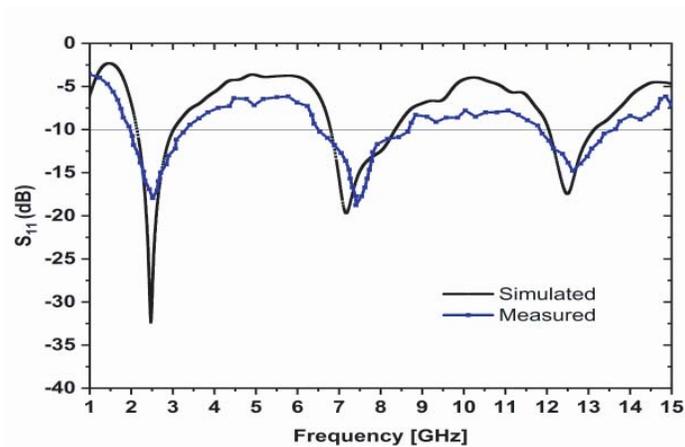(a)   (b)
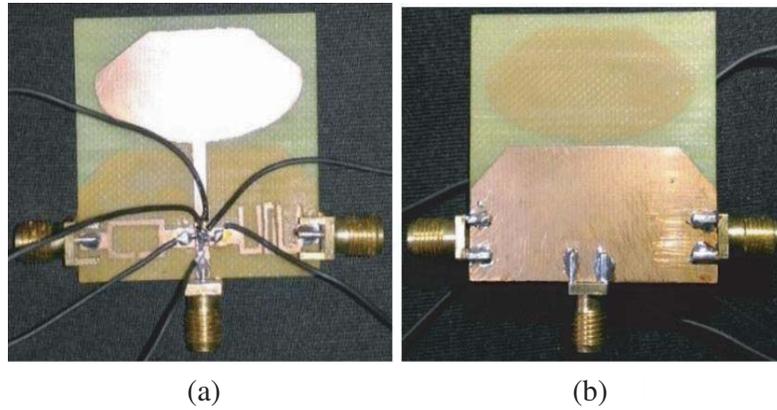
Figure 15. Fabricated antenna. (a) Front view. (b) Back view.
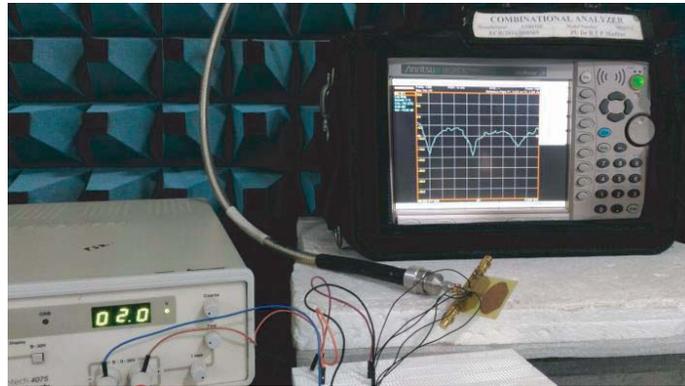
Figure 16. Measuring results in combinational analyzer.
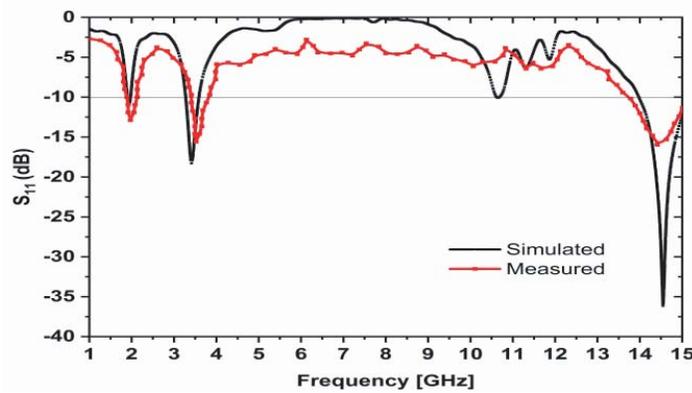

Figure 17. Comparison between simulation and measured result when D1 ON, D2 ON and D3 OFF.

4. SIMULATION AND MEASUREMENT RESULTS

4.1. Input Reflection Coefficient

The prototyped reconfigurable antenna is shown in Fig. 15. The antenna parameters are measured with a combinational analyzer in an anechoic chamber as shown in Fig. 16. The S_{11} of the proposed antenna is

Figure 18. Comparison between simulation and measured result when D1 OFF, D2 ON and D3 ON.

Table 3. Performance comparison of frequency re-configurable antenna.

Ref. No.	Type of Antenna	Var. No.	Frequency in GHz	Range of Tuning	Gain in dBi	Profile in mm	Size
[14]	Antenna with tunable feed network		2.6 to 3.35	25.2	-	12	1.3×1.3
[15]	Antenna with ferroelectric varactors	5	6.71 to 9.14	30.7	-3.1 to -5		0.22×0.22
[16]	Antenna with varactor diodes	2	2.14 to 3.33	43.5	1.1 to 2.4	0.8	0.29×0.17
[17]	Antenna with tunable FSS	20	2.26 to 2.75	19.6	3 to 5	5.32	0.6×0.6
[18]	Antenna with tunable FSS	112	1.1 to 1.54	33.3	-	10.8	0.63×0.63
[19]	Antenna with varactor diodes	2	1.92 to 2.1	8.9	-5 to 2	1.6	
[20]	Antenna with diode varactors	1	3.24 to 4.35	29.2	4 to 6.8	3.175	1.08×1.08
(This Work)	Truncated elliptical patch antenna	3	2.13 to 3.0 6.8 to 8.36 12.039 to 13.14	15.3	5.6 to 5.8	4.356	$0.33 * 0.31$

simulated and measured and shown in Fig. 17. When diode D1 is ON, D2 ON, and D3 OFF, we observe that the antenna operates at dual bands of 2.4 GHz and 12.1 GHz, respectively. When D1 is OFF, D2 ON, and D3 ON, we measure the reflection coefficient and compare the measured and simulated results as shown in Fig. 18. We obtain a good agreement between the simulated and measured results. The slight differences in the results are due to manufacturing errors, poor soldering, and Connector losses. A comparison between different reconfigurable antennas models and the designed antenna is presented in Table 3.
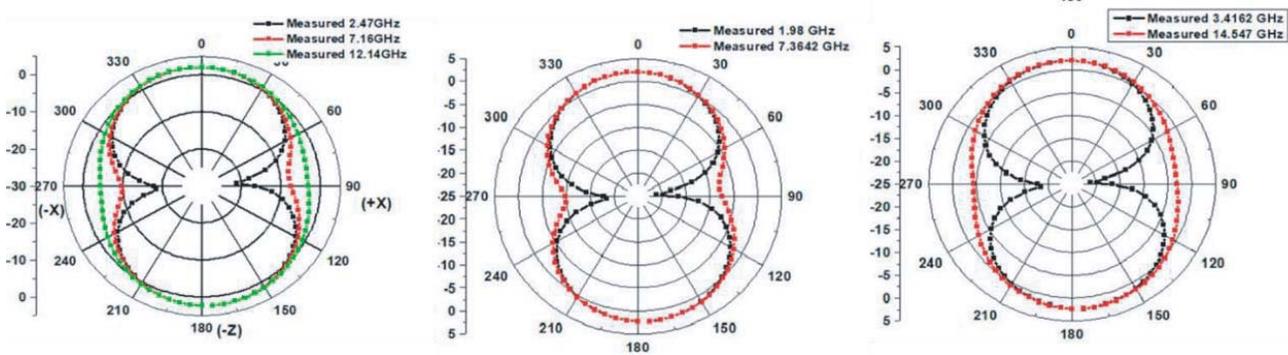
Figure 19. Radiation patterns.

4.2. Far Field Radiation Patterns

In the anechoic chamber, radiation patterns of the reconfigurable antenna are measured and evaluated. The measured radiation patterns for the fabricated antenna are shown in Fig. 19. The far field radiation patterns exhibit a high-performance shaped-beam behavior [23]. The radiation patterns in simulation and measurement are similar except small variations because of poor soldering and connector losses in the chamber.
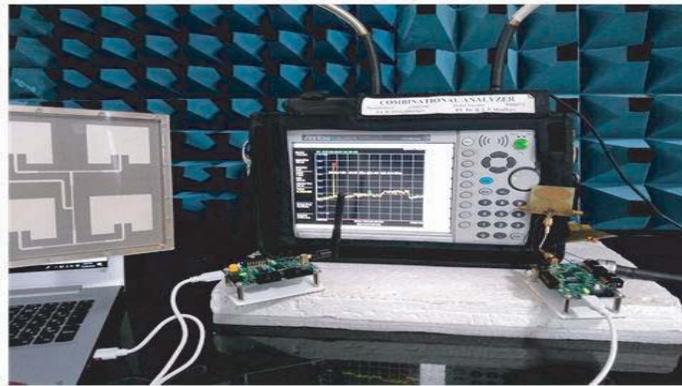
5. CONFIGURATION OF FABRICATED ANTENNA TO CDAC CMOTE DEVICE

Cmote is an embedded device developed by CDAC. It is used to transmit or receive data from one device to another. The Cmote device consists of one antenna that can operate at 2.4 GHz. Now in place of Cmote antenna, the fabricated antenna is connected and tested the antenna for validation in real time environment. We use two Cmote devices, a 2×2 array antenna, an ANRITSU MS2037C combinational analyzer, and a laptop. For one Cmote device, the fabricated antenna is connected, and for the other Cmote device, the default WHIP antenna is connected. Now both Cmote devices are powered by the Laptop. The combinational analyzer is operated in spectrum analyzer mode. It establishes the signal power at 2.4 GHz, which can be detected by a standard 2×2 array antenna which operates at the same frequency. When fabricated antenna is connected at receiver side, the switching elements of the fabricated antenna are biased to operate at 2.4 GHz.

The configuration of the fabricated antenna to the Cmote is shown in Fig. 20. The fabricated antenna is tested by using a combinational analyzer in spectrum analyzer mode. Data are transmitted from fabricated antenna to CDAC Cmote device, which can be observed from Fig. 21. The CDAC Cmote device is programable with user defined program for specific IoT application, and by using our fabricated antenna, we can transmit the information to another device to operate it as per the program.

Figure 20. Connecting fabricated antenna to CDAC Cmote.

Figure 21. Transmitting data from fabricated antenna to CDAC Cmote.

6. CONCLUSION

A reconfigurable antenna is presented to realize wideband-to-narrowband frequency reconfiguration using filtering function. Without increasing the size of the antenna, multi-functional characteristics are obtained in the antenna by using three p-i-n diodes. These p-i-n diodes are employed to switch the resonant frequencies, and through this process we achieve frequency reconfigurability. The proposed antenna is fabricated and tested with CDAC Cmote device in an anechoic chamber. The data are successfully transferred from one Cmote device to another Cmote device with the proposed antenna placement. The frequency reconfigurable behavior and real time testing make this proposed antenna more suitable for IoT and other wireless platform-based applications.

ACKNOWLEDGMENT

REFERENCES

1. Cheung, C. Y., J. S. Yuen, and S. W. Mung, "Miniaturized printed inverted-F antenna for internet of things: A design on PCB with a meandering line and shorting strip," *International Journal of Antennas and Propagation*, Vol. 2018, Article ID 5172960, 5 pages, 2018.

2. Awais, Q., H. T. Chattha, M. Jamil, Y. Jin, F. A. Tahir, and M. U. Rehman, "A novel dual ultrawideband CPW-fed printed antenna for Internet of Things (IoT) applications," *Wireless Communications and Mobile Computing*, 1–9, https://doi.org/10.1155/2018/2179571, 2018.

3. Bashir, U., K. R. Jha, G. Mishra, G. Singh, and S. K. Sharma, "Octahedron-shaped linearly polarized antenna for multi standar services including RFID and IOT," *IEEE Transactions on Antennas and Propagation*, Vol. 65, No. 7, 3364–3373, 2017.

4. T. Li, H. Zhai, X. Wang, L. Li, and C. Liang, "Frequency-reconfigurable bow-tie antenna for bluetooth, WiMAX, and WLAN applications," *IEEE Antennas and Wireless Propagation Letters*, Vol. 14, 171–174, 2015.

5. C. Sun, H. Zheng, L. Zhang, and Y. Liu, "A compact frequency-reconfigurable patch antenna for beidou (compass) navigation system," *IEEE Antennas and Wireless Propagation Letters*, Vol. 13, 967–970, 2014.

6. Qin, P.-Y., F. Wei, and Y. J. Guo, "A wideband-to-narrowband tunable antenna using a reconfigurable filter," *IEEE Transactions on Antennas and Propagation*, Vol. 63, No. 5, 2282–2285, 2015.

7. Rhee, C. Y., J. H. Kim, W. J. Jung, T. Park, B. Lee, and C. W. Jung, "Frequency-reconfigurable antenna for broadband airborne applications," *IEEE Antennas and Wireless Propagation Letters*, Vol. 13, 189–192, 2014.

8. Majid, H. A., M. K. A. Rahim, M. R. Hamid, and M. F. Ismail, "Frequency and pattern reconfigurable slot antenna," *IEEE Transactions on Antennas and Propagation*, Vol. 62, No. 10, 5339–5343, 2014.

9. Cai, Y.-M., K. Li, Y. Yin, S. Gao, W. Hu, and L. Zhao, "A low-profile frequency reconfigurable grid-slotted patch antenna," *IEEE Access*, Vol. 6, 36305–36312, 2018.

10. Majid, H. A., M. K. A. Rahim, M. R. Hamid, and M. Ismail, "A compact frequency-reconfigurable narrowband microstrip slot antenna," *IEEE Antennas and Wireless Propagation Letters*, Vol. 11, 616–619, 2012.

11. Han, T.-Y., Y.-J. Liao, et al., "A frequency reconfigurable half annular ring slot antenna design," *IEEE Transactions on Antennas and Propagation*, Vol. 62, No. 6, 3428–3431, 2014.

12. Yang, S. L. S., A. A. Kishk, and K. F. Lee, "Frequency reconfigurable U-slot microstrip patch antenna," *IEEE Antennas and Wireless Propagation Letters*, Vol. 7, 127–129, 2008.

13. Li, H.-Y., C.-T. Yeh, J.-J. Huang, C.-W. Chang, C.-T. Yu, and J.-S. Fu, "CPW-fed frequency reconfigurable slot-loop antenna with a tunable matching network based on ferroelectric varactors," *IEEE Antennas and Wireless Propagation Letters*, Vol. 14, 614–617, 2015.

14. Simorangkir, R. B., Y. Yang, K. P. Esselle, and B. A. Zeb, "A method to realize robust flexible electronically tunable antennas using polymer-embedded conductive fabric," *IEEE Transactions on Antennas and Propagation*, Vol. 66, No. 1, 50–58, 2018.

15. Cheung, S., Y. Cao, and T. Yuk, "Compact frequency reconfigurable slot antenna with continuous tuning range for cognitive radios," *2015 9th European Conference on Antennas and Propagation (EuCAP)*, 1–4, IEEE, 2015.

16. Costa, F., A. Monorchio, S. Talarico, and F. M. Valeri, "An active high-impedance surface for low-profile tunable and steerable antennas," *IEEE Antennas and Wireless Propagation Letters*, Vol. 7, 676–680, 2008.

17. Liang, B., B. Sanz-Izquierdo, E. A. Parker, and J. C. Batchelor, "A frequency and polarization reconfigurable circularly polarized antenna using active ebg structure for satellite navigation," *IEEE Transactions on Antennas and Propagation*, Vol. 63, No. 1, 33–40, 2015.

18. Sam, W. and Z. Zakaria, "The investigation of the varactor diode as tuning element on reconfigurable antenna," *2016 IEEE 5th Asia-Pacific Conference on Antennas and Propagation (APCAP)*, 13–14, IEEE, 2016.

19. Ge, L., M. Li, J. Wang, and H. Gu, "Unidirectional dual-band stacked patch antenna with independent frequency reconfiguration," *IEEE Antennas and Wireless Propagation Letters*, Vol. 16, 113–116, 2017.

20. Liu, W., Z. N. Chen, and X. Qing, "Metamaterial-based low-profile broad-band mushroom antenna," *IEEE Transactions on Antennas and Propagation*, Vol. 62, No. 3, 1165–1172, 2014.

21. Bahl, I. J. and P. Bhartia, *Microstrip Antennas*, Artech House, 1980.

22. Hong, J.-S. G. and M. J. Lancaster, *Microstrip Filters for RF/Microwave Applications*, Vol. 167, John Wiley & Sons, 2004.

23. Isernia, T. and A. F. Morabito, "Mask-constrained power synthesis of linear arrays with even excitations," *IEEE Transactions on Antennas and Propagation*, Vol. 64, No. 7, 3212–3217, 2016.